



TECHNICAL ARTICLE

Photoluminescent Plasma Electrolytic Oxidation Coatings Containing YAG: Ce Produced on 1050 Aluminum Alloy

Alessio Giorgio Settimi, Luca Pezzato, Alessandro Longato, Katya Brunelli, Alessandro Martucci, Silvia Gross, and Manuele Dabalà

Submitted: 14 March 2022 / Revised: 22 August 2022 / Accepted: 17 September 2022

In this work, we investigated the possible incorporation of YAG (yttrium aluminum garnet)-Ce particles into plasma electrolytic oxidation (PEO) coatings on 1050AA (aluminum alloy) in order to endow the surface with photoluminescent properties. Different treatment times and current modes (direct or pulsed) were tested as PEO process parameters using as electrolyte a silicates-containing solution. The microstructure of the samples was characterized by SEM and XRD measurements, the corrosion properties were determined by EIS tests, whereas the photoluminescence was evaluated with a proper spectrometer. The concentration of the YAG-Ce particles incorporated in the PEO coating was strongly influenced by the current mode, and in particular, it was higher with pulsed current mode. A higher content of YAG-Ce particles results in a better corrosion resistance and photoluminescent effect. PEO process in pulsed unipolar mode using an electrolyte containing YAG-Ce particles resulted an effective way to produce samples of 1050AA with a surface characterized by photoluminescent properties.

Keywords aluminum, coating, corrosion, photoluminescence, plasma electrolytic oxidation

1. Introduction

Plasma electrolytic oxidation (PEO) consists of a new surface conversion process, that is employed in order to enhance not only the mechanical, but also the surface properties of light alloys such as aluminum or magnesium (Ref 1-4). The process is similar to traditional anodization, however, it works with higher potential and current densities.

The key role in the process is played by micro-discharges on the surface of samples, formed due to the high voltage required in order to be above the dielectric breakdown. Indeed, these micro-discharges move randomly over the samples producing the growth of the oxide layer (Ref 5-8). The composition of the PEO coatings consists not only of the substrate oxides, but also of other oxides containing elements present in the electrolytes (Ref 9). The mechanism of formation of PEO coating and the influence of process parameters are well studied topics in the literature, focusing, for example, on light alloys (Ref 10-14) and steels (Ref 15). Thanks to its features, PEO coating can be employed in several applications where high mechanical and corrosion properties are required (Ref 16, 17). Another peculiarity of PEO coating is the possibility to incorporate into the coating different types of micro- or nanoparticles

coming from electrolytes without modifying the coating formation (Ref 18, 19). By this way, it is possible to functionalize the surface or confer tailored properties for different purposes. Various examples are presented in the literature, one of these concerns the use of silver or copper particles to provide antibacterial and fungicidal properties to the PEO coatings (Ref 20-22).

Rare-earth ion-doped materials, such as phosphor and other oxides, have a great scientific and technological interest due to their wide use in optoelectronic devices and applications. For example, phosphors are employed in the production of white led (Ref 23, 24). In particular, YAG:Ce exhibits absorption bands at 340 and 460 nm and a broad emission band in the visible spectra centered at 550 nm as a consequence of the $5d \rightarrow 4f$ transition (Ref 25). Recently, investigations showed that PEO is a very suitable process for obtaining coating light-emitting species (Ref 26-28). However, no works in the literature reported the incorporation of YAG:Ce particles into PEO coatings.

Another research branch consists of the variation in current mode during PEO treatments. The application of different electrical regimes with DC, pulsed DC, or AC power supply leads to obtain oxide coating with different properties, varying micro-discharges formation (Ref 29). In particular, it is possible to employ pulsed current instead of direct current. Indeed, it was demonstrated in the literature that, using DC, it is possible to obtain a thin PEO coating with a high porosity compared to ones achieved with pulsed current (Ref 30, 31). Pulsed current, instead, allows controlling micro-discharges on surface samples, leading to denser and thicker layers that improve corrosion resistance (Ref 32, 33).

In this work, the results concerning the addition of YAG:Ce particles directly in the electrolyte used to produce PEO coating on pure aluminum, in order to obtain an oxide coating with phosphors, are reported. Moreover, the influence of current mode (direct or pulsed current) on particle distribution into the coating and photoluminescence properties was investigated.

Alessio Giorgio Settimi, Luca Pezzato, Alessandro Longato, Katya Brunelli, Alessandro Martucci, and Manuele Dabalà, Department of Industrial Engineering, University of Padova, Via Marzolo 9, 35131 Padua, Italy; Silvia Gross, Department of Chemical Sciences, University of Padova, Via Marzolo 1, 35131 Padua, Italy. Contact e-mails: luca.pezzato@unipd.it and lucapezzato@virgilio.it.

This treatment could be very useful in the production of photoelectronic devices, such as light-emitting diodes, for both domestic and industrial applications. High-power lasers will be in fact employed in the future instead of LED, due to increase in the luminous efficacy, but this will cause higher heat generation in the point where the laser reaches the phosphor with problems of degradation of the phosphors. The use of substrates with high thermal conductivity, such as 1050 AA, with a modified phosphor-containing surface, like the one obtained with PEO process, can properly overcome this problem. In this work, a novel promising application of PEO process is presented, where YAG:Ce containing PEO coatings are for the first time produced, in order to obtain, on a substrate with high thermal conductivity, a phosphor-modified surface.

2. Experimental Details

2.1 PEO Samples Preparation

In this work, a 1050 aluminum alloy, whose nominal composition is reported in Table 1, was employed as substrate for PEO coating. 1050 AA was chosen; thanks to its high thermal conductivity in comparison with other aluminum alloys.

Before treatments, the samples were polished with abrasive papers (until 4000 grit) and degreased with acetone in ultrasounds for 10 min.

The polished substrates were PEO treated in an aqueous solution containing 25 g/l of Na_2SiO_3 and 2.5 g/l NaOH. For phosphors-containing PEO coating, 15 g/l of YAG:Ce commercial powder (NYAG4355 from Intematix), maintained in suspension thanks to magnetic stirring, were directly added into the electrolyte. Moreover, 0.2 g/l of sodium dodecyl sulfate ($\text{NaC}_{12}\text{H}_{25}\text{SO}_4$) was employed in the PEO solution as a surfactant to avoid powder agglomeration. The average size of YAG:Ce particles was 8.5 μm (Ref 34) and thanks to the presence of sodium dodecyl sulfate and magnetic stirring; they remain dispersed into the solution without precipitate.

The PEO process was carried out using a TDK-Lambda DC power supply of 2400 W (315 V, 8A). During the treatment, the aluminum samples worked as anode, while a carbon steel mesh was used as a cathode. The treatments in DC (Direct Current) mode were performed maintaining a constant current density of 0.4 A/cm², allowing the potential free to vary. In order to avoid the heating of the solution, a thermostatic bath was employed. For generating a pulsed PWM (pulse width modulation) signal, it was used a supply, based on a relay technology, that opens and closes an electric contactor. The frequency selected in the supply was 20 Hz, with a duty cycle of 50%. The treatments lasted for 5 or 10 min.

After the PEO treatment, the samples were washed with deionized water and ethanol and dried with compressed air. All the samples produced are summarized in Table 2. Two different current modes were selected for PEO treatments. In particular,

Table 1 Chemical composition in wt.% of 1050 alloy

Al%	Si%	Fe%
99.5	0.25	0.25

DC indicates PEO coating obtained with direct current, whereas UP indicates that unipolar pulsed current was employed for the coating production. In Table 2, the sample G was produced with the same electrical parameters of sample F but with a stronger magnetic stirring.

2.2 Samples Characterization

Firstly, the surfaces of different samples were observed with stereomicroscope Zeiss Stemi-C, in order to evaluate the presence of YAG:Ce powders and the external appearance of samples.

Then, the cross sections of the samples, after cutting operations, were mounted in epoxy resin and polished with standard metallographic technique (grinding with abrasive papers until 4000 grit and polishing with diamond suspension of 6 and 1 μm size). Both the surface and the cross section of treated samples were examined with a Cambridge Stereoscan 440 scanning electron microscope, equipped with a Philips PV9800 EDS. Moreover, to evaluate the distribution of YAG:Ce particles into the coating, EDS elemental mapping was performed on the cross section of one PEO + YAG:Ce sample.

In order to better evaluate the structure of the coating, x-ray diffraction (XRD) analyses were performed using a Phillips PW1710 diffractometer, with a nickel-filtered Cu-K α radiation source, operating at 30 kV and 40 mA, with a step size of 0.05, counting time of 6 s and a 2 θ range of 10 to 70°. The incident angle of the radiation was fixed to 3° in a thin-film mode.

Samples D and F, as more promising samples obtained with and without particles addition, were further investigated by XPS measurements with a Φ 5600ci Perkin-Elmer spectrometer, using a standard aluminum (Al K α) source, with an energy of 1486.6 eV operating at 200 W. The x-ray source employed was located at 54.7° relative to the analyzer axis. The working pressure was $< 5 \cdot 10^{-8}$ Pa - 10^{-11} torr. The calibration was based on the binding energy (B.E.) of the Au4f_{7/2} line at 83.9 eV with respect to the Fermi level. The standard deviation for the B.E. values was 0.15 eV. The reported B.E. was corrected for the B.E. charging effects, assigning the B.E. value of 284.6 eV to the C1s line of carbon. Survey scans were obtained in the 0-1350 eV. Detailed scans were recorded for relevant regions (O1s, C1s, Al2p, Si2p and Na1s, Al2s, Y3d, Y3p, Ce3d, Ce4d) depending on the examined sample. The atomic composition, after a Shirley-type background subtraction, was evaluated using sensitivity factors supplied by Perkin-Elmer. The samples were loaded onto the XPS sample holder by using conducting biadhesive tape. The acquired data were then interpreted with the use of the MultiPak software package. Assignment of the peaks was carried out according to the literature data (Ref 35) and to NIST database (Ref 36).

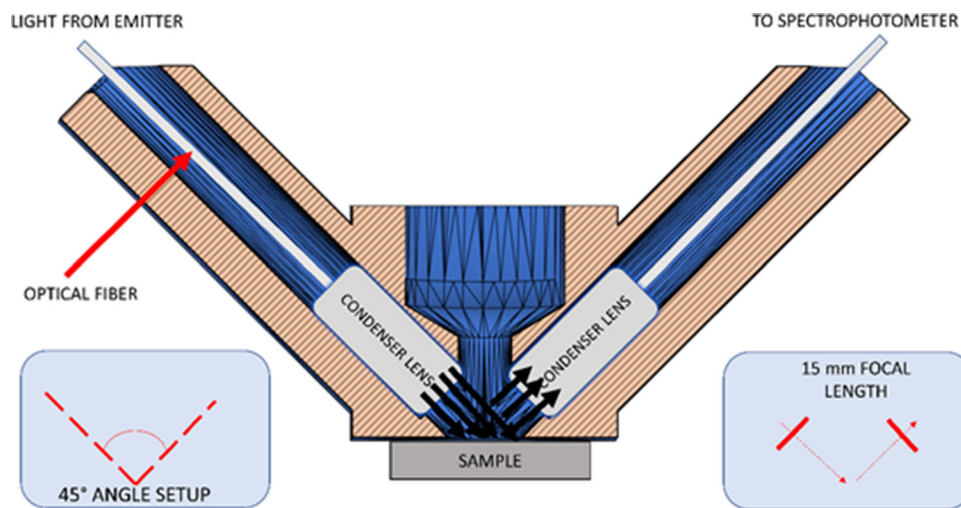
Photoluminescence (PL) properties were analyzed using an Ocean Optics HR4000 spectrophotometer measuring emissions spectra of samples. The setup, shown in Fig. 1, is formed by homemade (3D printed) measuring chamber and two optical fibers mounted in order to ensure a 90° alignment between the incident light and reflected light. The incident radiation is developed by a blue led (Ocean Optics Led) with 450 nm wavelength. The measurements were performed in triplicate to assure reproducibility.

2.3 Corrosion Resistance

The corrosion behavior of PEO-treated samples was evaluated with electrochemical impedance spectroscopy tests (EIS)

Table 2 Parameters employed for the production of PEO coatings on the different samples

Samples	Current mode	YAG:Ce particles	Surfactant	Treatment times	Magnetic stirring
A	DC	0 g/L	0 g/L	5 min	Moderate
B	DC	0 g/L	0 g/L	10 min	Moderate
C	UP	0 g/L	0 g/L	5 min	Moderate
D	UP	0 g/L	0 g/L	10 min	Moderate
E	DC	15 g/L	0.2 g/L	5 min	Moderate
F	UP	15 g/L	0.2 g/L	10 min	Moderate
G	UP	15 g/L	0.2 g/L	10 min	Strong

**Fig. 1** Homemade measuring chamber used for the PL measurements

and potentiodynamic polarization tests (PDP). EIS tests were performed at the open circuit potential (OCP), after 1 h of stabilization, with a materials instrument spectrometer connected with AMEL 2549 potentiostat using a frequencies range of 10^5 - 10^{-2} Hz and a perturbation amplitude of 10 mV. The setup of the EIS tests consists of a saturated calomel electrode (SCE) as reference electrode and a platinum electrode employed as a counter electrode. The composition of the electrolyte chosen was 0.1 M Na_2SO_4 and 0.05 M NaCl in order to simulate a moderate aggressive environment. The measures were performed in triplicate to assure reproducibility. The experimental data were then fitted with the software Z-View using a proper equivalent circuit. PDP tests were performed with the same setup and electrolyte employed for EIS test after 1 h of OCP stabilization. Tests were performed in a potential range between -1.7 and 0.5 V with a scan speed of 0.5 mV s^{-1} . Also, PDP tests were performed in triplicate in order to assure reproducibility and corrosion potentials and corrosion current densities were graphically extrapolated with the Tafel method.

3. Results and Discussion

3.1 Characterization

The PEO-treated samples with and without YAG:Ce were analyzed with a stereomicroscope. For PEO samples without

particles, samples B and D were selected because obtained with the same treatment times, but with different current regimes (Fig. 2). Sample B, obtained with DC, shows a different surface with respect to sample D produced with UP. Indeed, it is possible to observe that the surface of sample B shows more porosity and a higher roughness, while sample D is more smooth and homogeneous. The use of DC leads to an increase in the coating porosities rather than UP due to the difficulty of controlling the plasma micro-discharges (Ref 37, 38).

Concerning the samples obtained with YAG:Ce particles, we selected sample E (obtained in DC mode but with 5 min of treatment time, because with 10 min, the presence of particles and the DC mode do not permit to control the process) and sample F (obtained in UP current mode with 10 min of treatment time). The results are shown in Fig. 3.

From Fig. 3, it is possible to notice that there is the presence of a higher particle concentration together with a better distribution along the surface of sample F. In the sample produced with DC (sample E), instead, YAG:Ce particles are less uniformly distributed across the surface and tend to form big agglomerates.

Figure 4 reports SEM images of the cross section and the surface of the different samples produced without particle addition.

It is possible to observe that sample A shows a thick and quite uniform coating, with an average thickness of $45 \mu\text{m}$. The surface morphology is the typical one obtained for PEO coatings with this electrolyte composition. The coating shows a volcano-like morphology with a combination of nodular

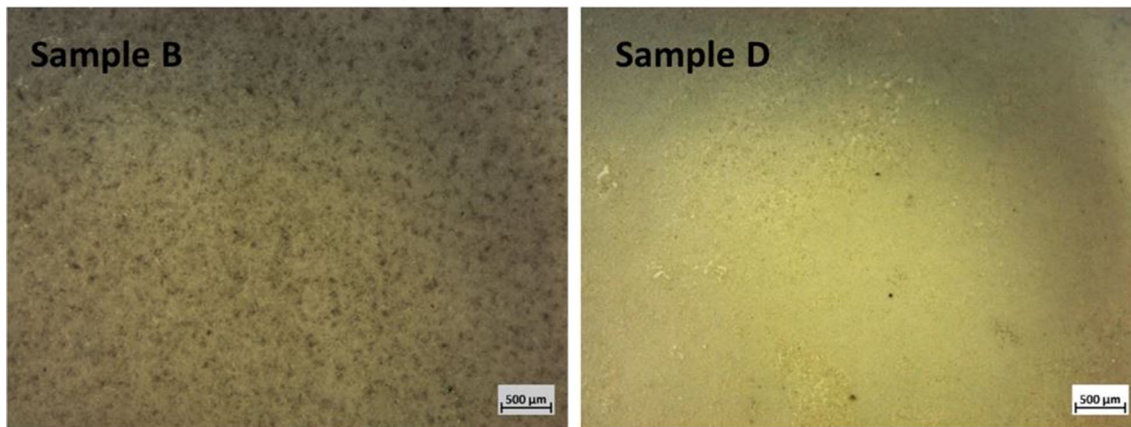


Fig. 2 Stereomicroscope images of the samples without particles obtained in DC mode (on the left) and UP mode (on the right)

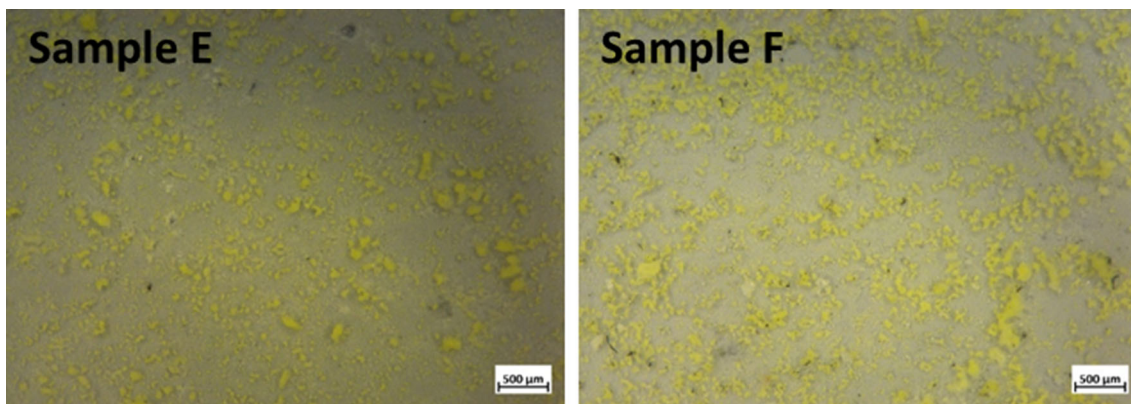


Fig. 3 Stereomicroscope images of the samples with particles obtained in DC mode (on the left) and UP mode (on the right)

particles and craters distributed over the surface, with non-uniform distribution of micropores, micro-cracks and porosities (Ref 39). The cross-sectional image shows deep channels and open pores (pancakes) (Ref 39). These structures arise from gas bubbles generating during PEO processes. Increasing the treatment time, the coating improves its features for a PEO process with DC. Indeed, the coating in sample B is more adherent, with increased thickness of $68\ \mu\text{m}$, and less porous.

Sample C, instead, shows how employing UP is possible to obtain a coating with small porosities well distributed along the surface and a thickness of $40\ \mu\text{m}$. In this way, the coating appears denser with a limited volcano-like morphology. By increasing the treatment time, as shown for sample D, there is the formation of a high number of porosities compared to sample C and an increase in the coating thickness that reaches an average value of $80\ \mu\text{m}$.

Figure 5 reports SEM images of cross sections and surfaces of samples obtained with the addition of YAG:Ce particles in the solution. It can be first of all observed a remarkable reduction in the thickness of the PEO coatings in comparison with the ones obtained without particles addition. This fact can be linked with the modification in the discharge phenomena, due to the semiconductor nature of YAG:Ce, and with the fact that, as reported in the literature (Ref 40), oxide particles are not efficient to enhance the thickness of coating that generally got thinner by adding oxide particles.

The sample E, obtained with DC, shows a non-uniform and very thin coating (thickness of $9\ \mu\text{m}$), with a very high number

of porosities. It is possible also to observe zones with a high concentration of YAG:Ce particles and others without particles. Concerning sample F, achieved with UP, the coating is thin ($\sim 10\ \mu\text{m}$) with lower porosities compared to sample E. Moreover, there are evident white zones along the surface which highlight the presence of large quantities of YAG:Ce particles near and inside porosities. Concerning sample G (similar to sample F but obtained with higher stirring rate of electrolyte solution), the coating is also in this case $\sim 10\ \mu\text{m}$ thick, but it is possible to recognize the presence of a rather extended white zone outlining that YAG:Ce particles were incorporated into coating porosities. However, the surface analysis shows that the particles distribution is better in sample F rather than sample G, where phosphors tend to form big aggregates.

From the above-reported analysis, it is possible to conclude that the quantity of incorporated particles is strongly influenced by the current mode, and in particular, it is increased when UP is used, even if direct comparison is difficult due to the different treatment time between sample E and samples F/G. This can be probably linked to the fact, reported by Clyne et al. (Ref 29), that the discharge phenomena are more controlled with the UP current. In this way, in fact, the particles can remain into the discharge channels without being expelled by strong gas production, that is instead typical of PEO coatings produced in DC mode (Ref 41).

In order to evaluate the distribution of YAG:Ce particles and to understand if its presence is only almost superficial or also

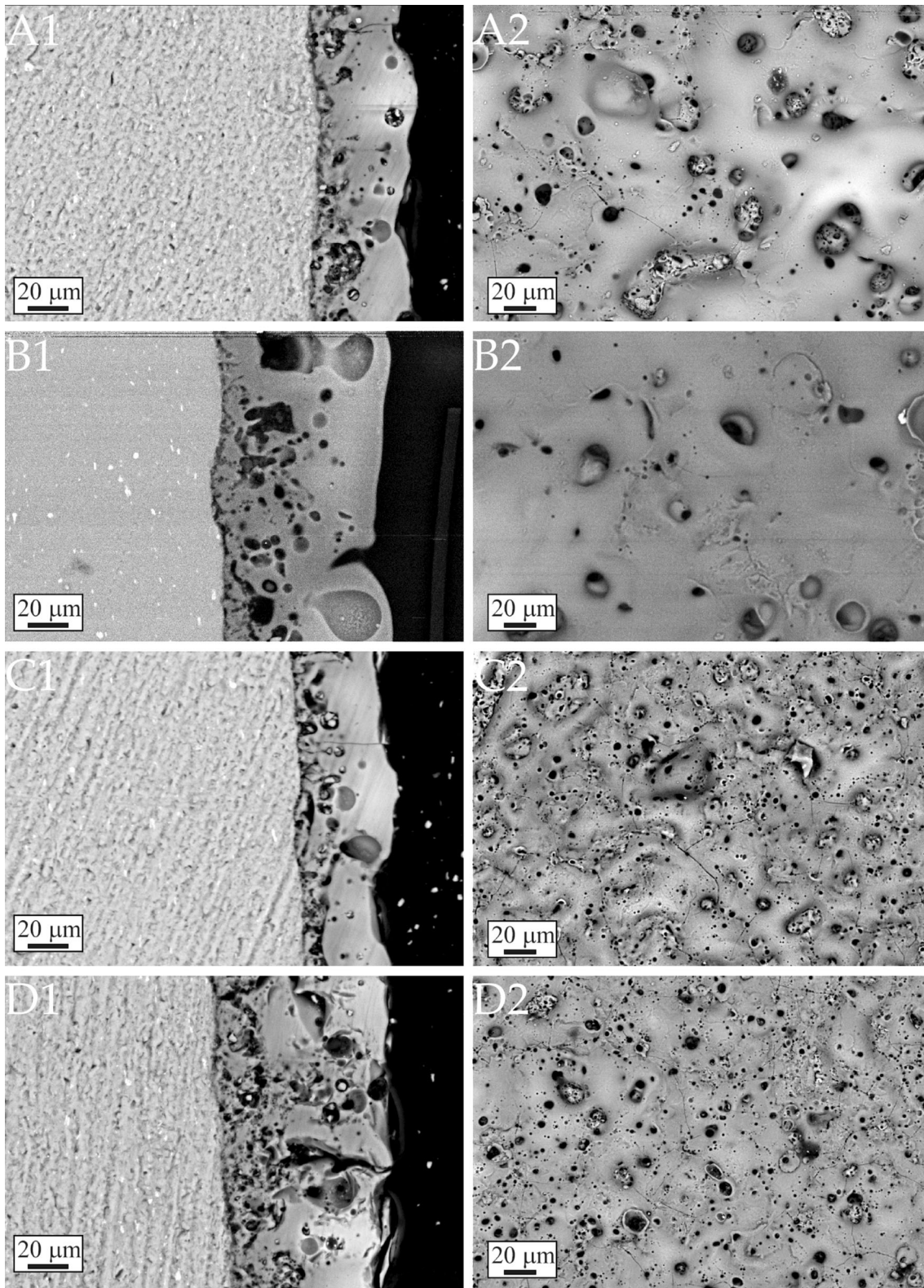


Fig. 4 SEM microstructures of cross section (left) and surface (right) of the samples without particle addition

inside coating, EDS elemental mapping was performed along the cross section of sample F and the results are reported in Fig. 6. Sample F was selected to perform EDS elemental mapping due to the fact that it seems the one with the higher quantity and best distribution of YAG:Ce particles.

From the SEM image, the presence of YAG:Ce particles (white spots) can be clearly noted not only on the surface, but also inside the coating. This fact is shown also from elemental mapping, where it can be observed that yttria (the main component of particles) is present also in coating, that is mainly

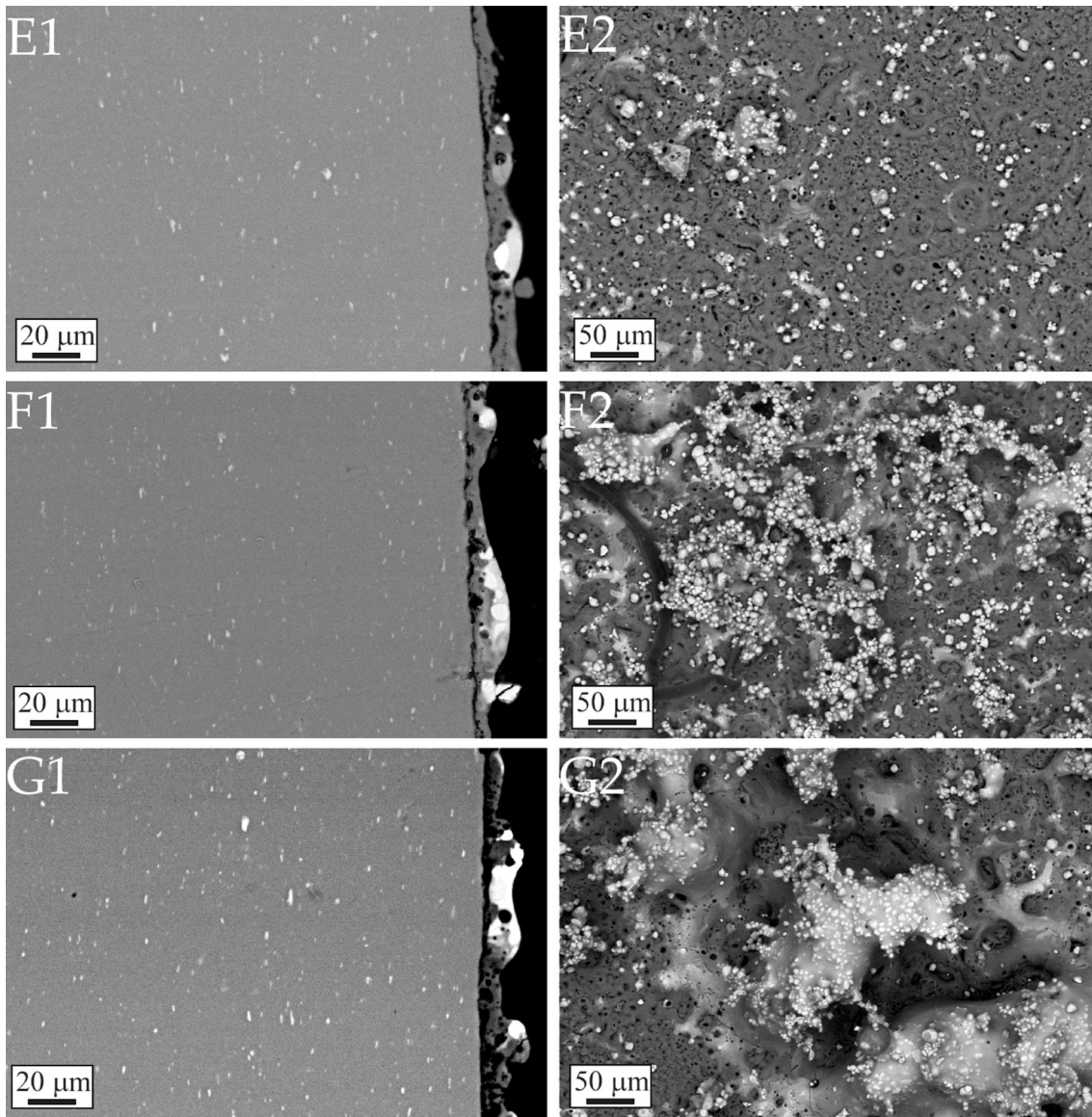


Fig. 5 SEM microstructures of cross sections (left) and surfaces (right) of samples with YAG:Ce particles addition

formed by Al, Si and O. Particles distribution on surface and inside coating is in accordance with other previous work (Ref 42). In particular, also in this case, the main incorporation mechanism consists of sweeping of particulate into the pores linked to active discharge sites refilled with electrolyte immediately after plasma collapse. Moreover, particles could decorate the free surface of the coating fairly uniformly at the end of the process due to sedimentation.

In order to better verify the composition of coating, SEM-EDS elemental analyses were performed on the surface of samples both with and without particles: The results are reported in Fig. 7.

In Fig. 7(A), the EDS spectra of surface of sample D, that has no particle inside, are reported. It can be observed that the coating is just formed by Al, Si and O, in agreement with the chemical composition of the substrate (Al 1050 alloy) and of the electrolytic solution which is composed by silicates. Figure 7(B), instead, shows EDS spectra of sample F with particle addition. It is clear that, besides of Si, Al and O peaks,

the presence of Y peak confirms the incorporation of a large amount of phosphor particles inside the coating.

To analyze more in detail the phase composition of the coating, XRD analyses were performed and the results are reported in Fig. 8.

It is possible to observe that, besides peaks related to aluminum (coming from the substrate, PDF-2 reference number N°00-004-0787), the coating is mainly formed by silica (SiO_2 , PDF-2 reference number N°00-050-1432), corundum (Al_2O_3 , PDF-2 reference number N°00-046-1212) and kyanite (Al_2SiO_5 , PDF-2 reference number N°00-087-1708), that are typical compounds occurring when the PEO process is developed on aluminum alloys with electrolytes based on silicates (Ref 20, 43, 44). Moreover, in samples treated with particles, it is evident that the presence of YAG GARNET ($\text{Y}_3\text{Al}_5\text{O}_{12}$, PDF-2 reference number N°00-033-0040) is related to the phosphors particles.

XPS survey scans (in the 0–1300 eV binding energy range, Fig. 9) were initially carried out on the samples to rule out the

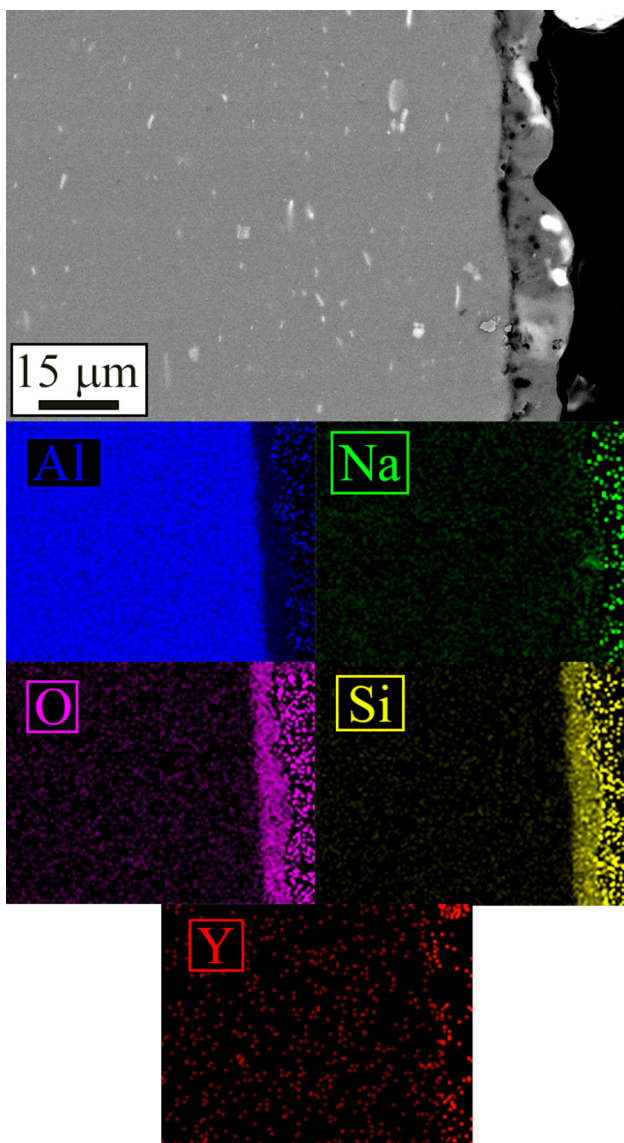


Fig. 6 SEM-EDS elemental mapping performed on the cross section of sample F containing YAG:Ce particles

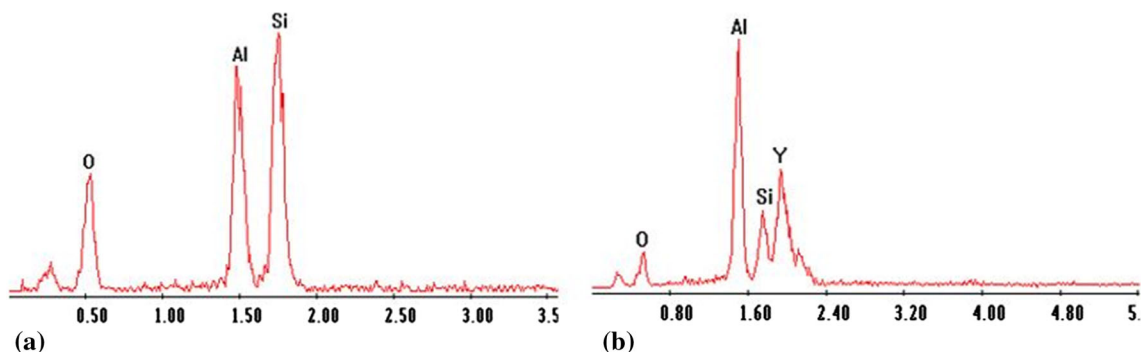


Fig. 7 SEM-EDS spectra performed on the surface of sample D without particles addition (A) and sample F with particles inside coating (B)

presence of any impurities or the presence of components beyond the expected composition. Based upon the results obtained by a preliminary survey scan, high-resolution spectra were collected from the regions of interest (C, O, Al, Na, Si, Y and Ce). From these spectra, it was possible to obtain quantitative data on the surface composition of the samples (Table 3). The presence of C is due to adventitious contamination and was used for referencing purposes to correct for charging effects.

Also, high-resolution single-peak fitting analysis was performed on the sample F for the Y3p peak in order to more deeply investigate the presence of phosphors on the PEO-coated surface. The results are reported in Fig. 10 even if Y3p peak analysis was complicated by the proximity of the Mg KLL peak (the Y3d region was unusable due to actual overlap with the much more intense Si2s peak). The calculated binding energies (311.5 eV) are compatible with $\text{Al}_5\text{O}_{12}\text{Y}_3$, YAG Garnet, (Ref 34, 35), confirming the results of XRD analysis where this compound was found in the samples produced with phosphor particles.

3.2 Photoluminescence Properties

Figure 11 shows the PL spectra of PEO samples with and without the addition of YAG:Ce particles in solution. These spectra have been integrated from 520 to 650 nm, this value is directly correlated to the quantity and homogeneity of YAG:Ce deposited on the substrate.

The spectrum of sample D, as all the samples without phosphors in the solution, presents only the scattered blue LED light. The samples E, G and F all exhibit a broad peak centered at 550 nm, due to PL emission from the YAG:Ce phosphors, which means that all of them incorporated phosphor in the matrix. Sample F presents the higher PL intensity value, 1.5 times higher than sample G and 2.3 higher than sample E. These results are in agreement with the SEM analysis: Low yield of sample E is probably due to the low concentration of phosphor on the coating obtained with the DC treatment. Both samples F and G were treated with UP, but the greater stirring of the electrolyte in sample G formed big aggregates of phosphor, whereas the sample F is more homogeneous, thus giving a higher yield in PL. The results of this analysis indicate

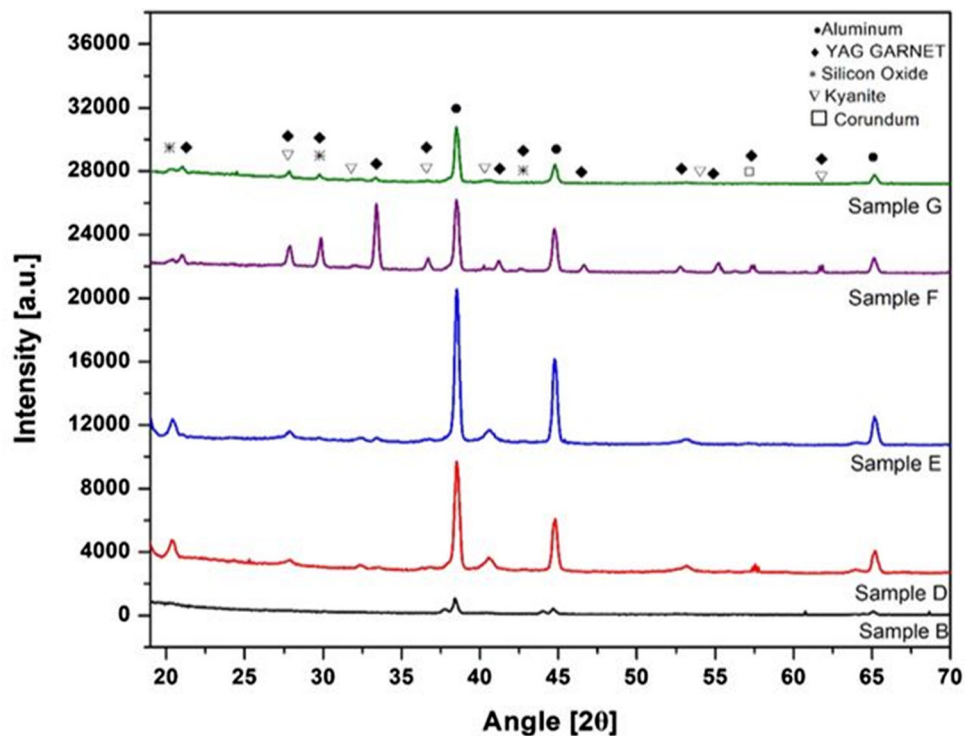


Fig. 8 XRD pattern of PEO coatings treated with and without the addition of YAG:Ce particles

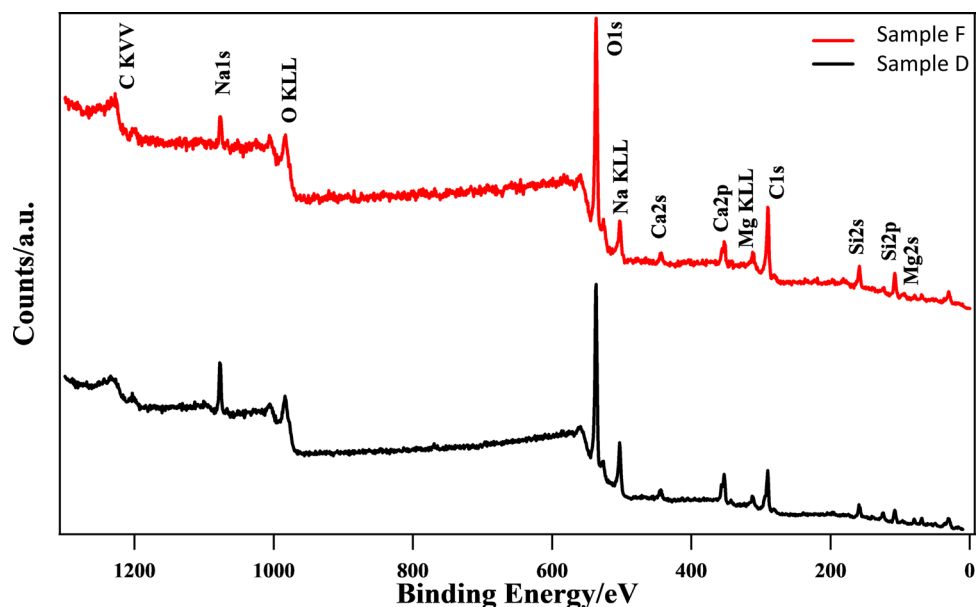


Fig. 9 Survey scans collected from the samples with main peaks indexed. Binding energies not corrected for surface charging. Minor and less visible peaks were not indexed

that it is possible to tune the PEO coating parameters to get a suitable matrix for the incorporation of YAG:Ce³⁺ phosphor.

3.3 Corrosion Resistance

The corrosion resistance of all samples was investigated through EIS tests in a solution containing sulfates and chlorides. The results in terms of Nyquist plot are shown in Fig. 12.

Experimental data of EIS tests were fitted employing Z-View software, using the equivalent circuit reported in Fig. 13. This is a circuit often employed to fit EIS data of PEO samples, because permit to consider the presence of an inner layer, that gives the major protection against corrosion, and an external porous layer (Ref 45).

In detail, R₁ represents the resistance of electrolyte, whereas the two parallels consider the interfaces formed between

Table 3 Surface composition (atomic %) of the analyzed samples

Sample	C	O	Al	Na	Si	Y	Ce
Sample F	37.7	46.6	1.5	3.9	10.3	0.1	0.0
Sample D	28.3	50.7	4.8	8.7	7.5	N/A	N/A

electrolyte and the two layers of PEO coating. In particular, R_2 -CPE₁ describes the interface between the outer and porous layer and electrolyte, while R_3 -CPE₂ represents the interface between electrolyte into pores and the inner dense layer that acts as a barrier in PEO coatings. The fitting results of experimental data are reported in Table 4. Good fitting quality was obtained in agreement with the low reported values of chi-squared and the good agreement between dots and lines in Fig. 12.

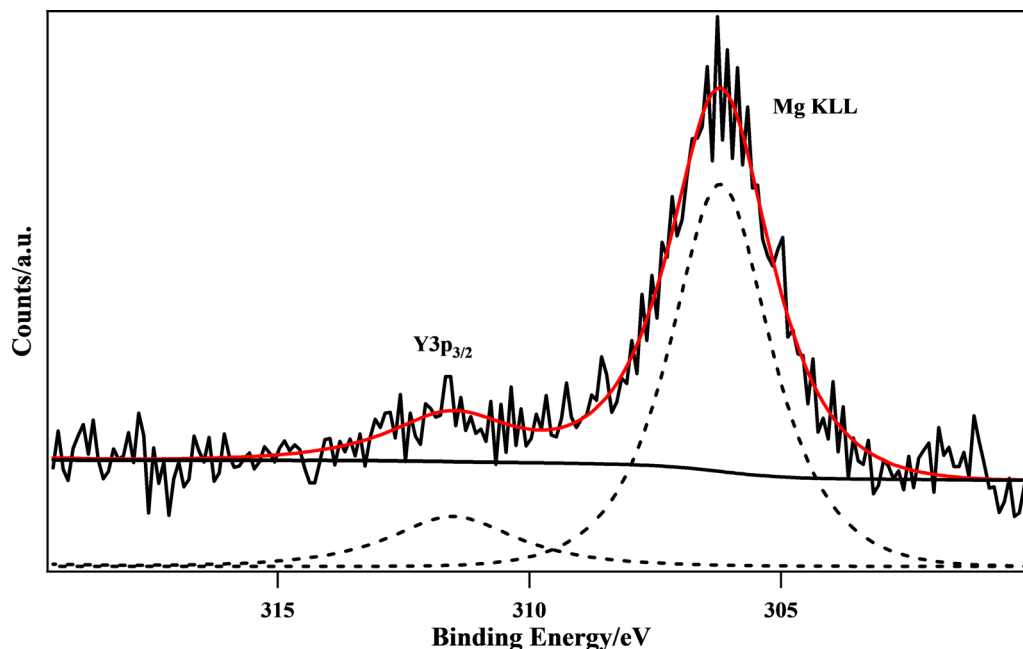


Fig. 10 High-resolution single-peak spectra of the Y3p region in sample F. Binding energies corrected for surface charging

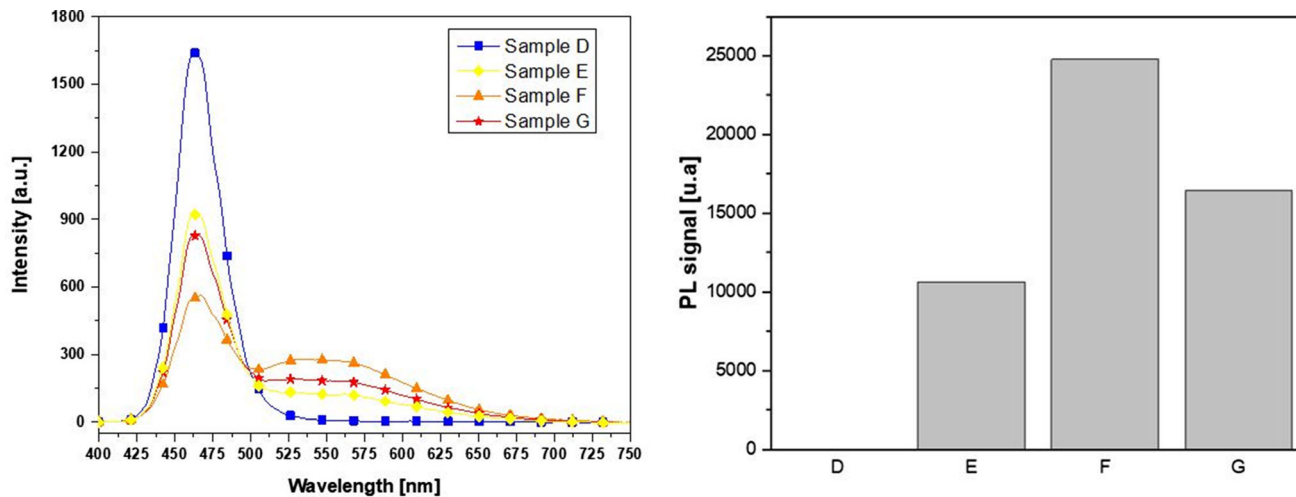


Fig. 11 PL spectra of PEO samples with and without the addition of YAG:Ce particles in solution (left). Integrated photoluminescence from 520 to 650 nm of the spectra (right)

Concerning the Nyquist plots reported in Fig. 12, it is possible to observe that sample treated with UP current with the incorporation of YAG:Ce particles (sample F) is characterized by improved corrosion resistance compared to all the other samples. Indeed, considering the width of the semicircle and the intersection with X-axis at low frequencies as a qualitative way to evaluate the polarization resistance R_p , an increase of more than one order of magnitude in polarization resistance can be observed in sample F compared to all the other samples. Considering the inset in Fig. 12, the samples obtained with direct current mode and particles addition are characterized by a higher polarization resistance compared to the corresponding samples without particles.

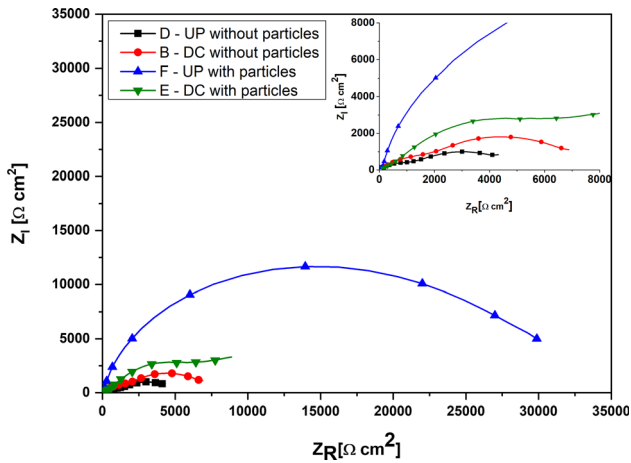


Fig. 12 Nyquist plot of samples obtained employing direct and pulsed current with and without the addition of YAG:Ce particles in solution. Dots represent experimental data and lines the result of the fitting. Test electrolyte: 0.1 M Na₂SO₄ and 0.05 M NaCl

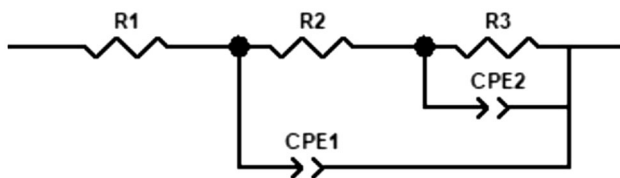


Fig. 13 Equivalent circuit employed for fitting EIS data for PEO-coated samples. It is possible to recognize two circuits that describe the inner and the outer layers that characterize PEO coating

Table 4 Results of the fitting of experimental data

Parameters	DC without particles	DC with particles	UP without particles	UP with particles
R_1 ($\Omega \text{ cm}^2$)	20.15	22.11	25.6	23.22
R_2 ($\Omega \text{ cm}^2$)	224.4	203	272.7	226.9
R_3 ($\Omega \text{ cm}^2$)	7830	15,030	6780	29,673
n_1	0.88	0.81	0.88	0.89
Q_1 ($\text{F cm}^{-2} \text{ Hz}^{1-n}$)	$7.33 \cdot 10^{-9}$	$1.99 \cdot 10^{-7}$	$6.87 \cdot 10^{-9}$	$8.09 \cdot 10^{-8}$
n_2	0.69	0.59	0.56	0.88
Q_2 ($\text{F cm}^{-2} \text{ Hz}^{1-n}$)	$1.33 \cdot 10^{-5}$	$4.16 \cdot 10^{-5}$	$5.14 \cdot 10^{-5}$	$6.20 \cdot 10^{-7}$
Chi-square	0.003	0.004	0.001	0.002

From the analysis of the fitting of the experimental data (Table 4), it is confirmed that the samples obtained with the addition of YAG:Ce particles, regardless the current mode, were characterized by improved corrosion performance in comparison with the corresponding samples without particles, as evidenced by the increased value of R_3 that is one order of magnitude higher in the samples without particles. Employing UP current further improves the corrosion resistance, in terms of R_3 , in the sample with YAG:Ce particles addition. This can be linked with a more homogeneous and uniform coating, as resulted by SEM observation.

The recorded corrosion behavior can be explained with the presence of YAG:Ce particles that fill the pores of PEO outer

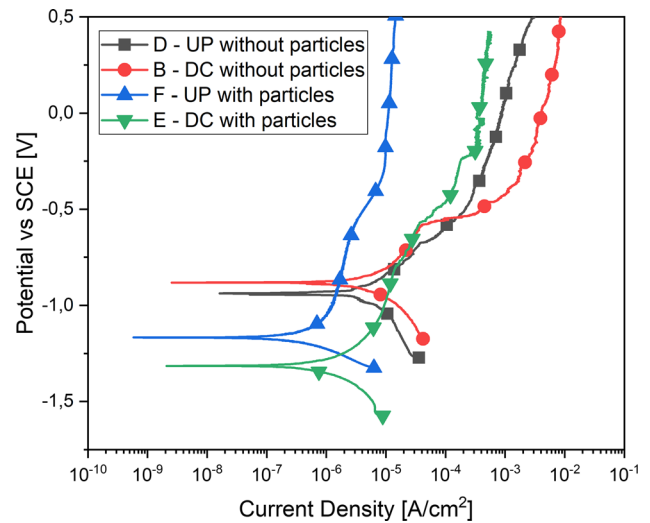


Fig. 14 Potentiodynamic polarization plot for the different PEO-treated samples. Test electrolyte: 0.1 M Na₂SO₄ and 0.05 M NaCl

Table 5 Corrosion potentials and corrosion current densities graphically extrapolated from potentiodynamic polarization tests

Sample	Corrosion potential, V	Current density, A/cm ²
D-UP without particles	- 0.94	$7.3 \cdot 10^{-6}$
B-DC without particles	- 0.88	$2.0 \cdot 10^{-5}$
F-UP with particles	- 1.17	$3.2 \cdot 10^{-7}$
E-DC with particles	- 1.32	$1.0 \cdot 10^{-6}$

layer producing an increase in the value of R_3 (that represent the interface between electrolyte into pores and the inner dense layer) since the filled pores do not allow the electrolyte to reach the substrate (Ref 40, 46). The impact of the porous layer is not so relevant to corrosion resistance, as evidenced by the fact that the R_2 values of all samples are similar. Moreover, the results of the corrosion tests are in accordance with the SEM observation; in fact sample F, the one with the best corrosion properties, is the one characterized by the presence of the thicker and more compact protective layer and by the higher quantity of particles incorporated into the coating.

In order to confirm the results of the EIS tests, also, potentiodynamic polarization tests (PDP) were performed and the results are reported in Fig. 14 and Table 5.

Considering the data coming from PDP tests, these substantially confirm the ones of EIS. The corrosion current density is directly connected to the corrosion rate and a decrease in the corrosion current density indicates an increase in the corrosion resistance. As can be noted, the sample characterized by the lower value of I_{corr} (one order of magnitude lower than the others, in the order of 10^{-7}) is the sample UP with particles, that was the one characterized by the higher value of polarization resistance R_3 in the EIS tests. The sample with the higher value of corrosion current density, in the order of 10^{-5} , is instead the sample DC without particles.

4. Conclusion

PEO-coated surfaces with PL properties were successfully obtained on 1050AA through direct addition of YAG:Ce particles into the electrolyte used during PEO process. In particular, it is possible to conclude that

- PEO coatings, without particles addition, showed higher thickness and uniformity employing UP current compared to direct current. With YAG:Ce particles addition, instead, PEO coating has a lower thickness compared to the ones without particles.
- Particles incorporation resulted strongly affected by the current mode. In particular, in the sample obtained with DC, a lower number of particles is incorporated into PEO coating and their distribution is less uniform. This is because DC does not enable a good control of discharges formation during PEO process. With UP current, instead, a higher number of YAG:Ce particles are incorporated with also a more uniform distribution.
- XRD patterns showed the presence of the typical phases of PEO coating such as silica (SiO_2), corundum (Al_2O_3) and kyanite (Al_2SiO_5), as well as YAG:Ce particles.
- PL measurements highlighted that the intensity of the scattering peak is higher for the sample obtained with UP current (sample F) compared to the ones with DC, due to the increase in the number of incorporated particles.
- The sample obtained in UP current mode with particle addition was the one with the best corrosion properties, both from EIS and PDP tests. This was related to the fact that the particles fill the pores of the coating, avoiding the electrolyte to reach the substrate and due to the fact that the coating obtained with pulsed current is denser in comparison with the one obtained with direct current.
- The addition of YAG:Ce particles in the electrolyte, to-

gether with a UP current mode, seems a promising way to produce photoluminescent and corrosion-resistant surfaces on substrates with high thermal conductivity that can be employed in photoelectronic devices, such as light-emitting diodes. The use of substrates with high thermal conductivity such as 1050AA will permit in fact to use high-power laser source without causing phosphor degradation and permitting to reach higher luminous efficacy.

Acknowledgments

Dr. Stefano Diodati (*Department of Chemical Sciences, University of Padova*) is gratefully acknowledged for valuable support in elaboration of XPS data.

Funding

Open access funding provided by Università degli Studi di Padova within the CRUI-CARE Agreement. Project supported by the BIRD 2020 program of the University of Padova (Project BIRD202558/20).

Open Access

This article is licensed under a Creative Commons Attribution 4.0 International License, which permits use, sharing, adaptation, distribution and reproduction in any medium or format, as long as you give appropriate credit to the original author(s) and the source, provide a link to the Creative Commons licence, and indicate if changes were made. The images or other third party material in this article are included in the article's Creative Commons licence, unless indicated otherwise in a credit line to the material. If material is not included in the article's Creative Commons licence and your intended use is not permitted by statutory regulation or exceeds the permitted use, you will need to obtain permission directly from the copyright holder. To view a copy of this licence, visit <http://creativecommons.org/licenses/by/4.0/>.

References

1. L. Pezzato, D. Vranescu, M. Sinico, C. Gennari, A.G. Settimi, P. Pranovi, K. Brunelli, and M. Dabalà, Tribocorrosion Properties of PEO Coatings Produced on AZ91 Magnesium Alloy with Silicate- or Phosphate-Based Electrolytes, *Coatings*, 2018, **8**(6), p 202
2. Q. Li, J. Liang, and Q. Wang, Plasma Electrolytic Oxidation Coatings on Lightweight Metals, *Mod. Surf. Eng. Treat.*, 2013, **4**, p 75–99. <https://doi.org/10.5772/55688>
3. F.H. Cao, L.Y. Lin, J.Q. Zhang, and C.N. Cao, Environmental Friendly Plasma Electrolytic Oxidation of AM60 Magnesium Alloy and Its Corrosion Resistance. *Trans. Nonferrous Met. Soc. China*, 2008, **18**(2), p 240–247
4. L.O. Snizhko, A.L. Yerokhin, A. Pilkington, N.L. Gurevina, D.O. Misnyankin, A. Leyland, and A. Matthews, Anodic Processes in Plasma Electrolytic Oxidation of Aluminium in Alkaline Solutions, *Electrochim. Acta*, 2004, **49**(13), p 2085–2095
5. J. Martin, A. Melhem, I. Shchedrina, T. Duchanoy, A. Nominé, G. Henrion, T. Czerwiec, and T. Belmonte, Effects of Electrical Parameters on Plasma Electrolytic Oxidation of Aluminium, *Surf. Coat. Technol.*, 2013, **221**, p 70–76. <https://doi.org/10.1016/j.surfcoat.2013.01.029>
6. F.H. Cao, J.L. Cao, Z. Zhang, J.Q. Zhang, and C.N. Cao, Plasma Electrolytic Oxidation of AZ91D Magnesium Alloy with Different

- Additives and Its Corrosion Behavior, *Mater. Corros.*, 2007, **58**(9), p 696–703
7. N. Xiang, R.G. Song, H. Li, C. Wang, Q.Z. Mao, and Y. Xiong, Study on Microstructure and Electrochemical Corrosion Behavior of PEO Coatings Formed on Aluminum Alloy, *J. Mater. Eng. Perform.*, 2015, **24**(12), p 5022–5031
 8. N. Xiang, R.G. Song, J.J. Zhuang, R.X. Song, X.Y. Lu, and X.P. Su, Effects of Current Density on Microstructure and Properties of Plasma Electrolytic Oxidation Ceramic Coatings Formed on 6063 Aluminum Alloy, *Trans. Nonferrous Met. Soc. China*, 2016, **26**(3), p 806–813. [https://doi.org/10.1016/S1003-6326\(16\)64171-7](https://doi.org/10.1016/S1003-6326(16)64171-7)
 9. T. Hryniewicz, Plasma Electrolytic Oxidation of Metals and Alloys. *Metals*, 2018, **8**, p 1058. <https://doi.org/10.3390/met8121058>
 10. M. Echeverry-Rendón, O. Galvis, R. Aguirre, S. Robledo, J.G. Castaño, and F. Echeverría, Modification of Titanium Alloys Surface Properties by Plasma Electrolytic Oxidation (PEO) and Influence on Biological Response, *J. Mater. Sci. Mater. Med.*, 2017 <https://doi.org/10.1007/s10856-017-5972-x>
 11. H. Soliman and A.S. Hamdy, Effect of Fluoride Ions Modifier and Ceramic Al₂O₃ Particles Additives on Plasma Electrolytic Oxidation of AZ31, *Surf. Eng.*, 2017, **33**(10), p 767–772. <https://doi.org/10.1080/02670844.2016.1214407>
 12. A. Sharma, Y.J. Jang, and J.P. Jung, Effect of KOH to Na₂SiO₃ Ratio on Microstructure and Hardness of Plasma Electrolytic Oxidation Coatings on AA 6061 Alloy, *J. Mater. Eng. Perform.*, 2017, **26**(10), p 5032–5042
 13. A. Khakzad, S.M. MousaviKhoi, S.A. Tayebifard, E. Aghaie, Y. Behnamian, M. Mozammel, and H. MalekiGhaleh, Alumina-Silica Composite Coatings on Aluminum by Plasma Electrolytic Oxidation: The Effect of Coating Time on Microstructure Phase and Corrosion Behavior, *J. Mater. Eng. Perform.*, 2017, **26**(6), p 2663–2670
 14. L. Pezzato, K. Brunelli, and M. Dabalà, Corrosion Properties of Plasma Electrolytic Oxidation Coated AA7075 Treated Using an Electrolyte Containing Lanthanum-Salts, *Surf. Interface Anal.*, 2016, **48**(8), p 729–738
 15. W. Yang, Q. Li, C. Liu, J. Liang, Z. Peng, and B. Liu, A Comparative Study of Characterisation of Plasma Electrolytic Oxidation Coatings on Carbon Steel Prepared from Aluminate and Silicate Electrolytes, *Surf. Eng.*, 2018, **34**(1), p 54–62. <https://doi.org/10.1080/02670844.2017.1320862>
 16. L. Ceschini, A. Morri, V. Angelini, and S. Messieri, Fatigue Behavior of the Rare Earth Rich EV31A Mg Alloy: Influence of Plasma Electrolytic Oxidation, *Metals Basel*, 2017, **7**(6), p 1–14
 17. B. Mingo, R. Arrabal, M. Moledano, Y. Llamazares, E. Matykina, A. Yerokhin, and A. Pardo, Influence of Sealing Post-Treatments on the Corrosion Resistance of PEO Coated AZ91 Magnesium Alloy, *Appl. Surf. Sci.*, 2018, **433**, p 653–667. <https://doi.org/10.1016/j.apsusc.2017.10.083>
 18. X. Lu, M. Moledano, C. Blawert, E. Matykina, R. Arrabal, K.U. Kainer, and M.L. Zheludkevich, Plasma Electrolytic Oxidation Coatings with Particle Additions—A Review, *Surf. Coat. Technol.*, 2016, **307**, p 1165–1182. <https://doi.org/10.1016/j.surfcoat.2016.08.055>
 19. L. Pezzato, L. Lorenzetti, L. Tonelli, G. Bragaglia, M. Dabalà, C. Martini, and K. Brunelli, Effect of SiC and Borosilicate Glass Particles on the Corrosion and Tribological Behavior of AZ91D Magnesium Alloy after PEO Process, *Surf. Coat. Technol.*, 2021, **428**(August), p 127901
 20. P. Cerchier, L. Pezzato, C. Gennari, E. Moschin, I. Moro, and M. Dabalà, PEO Coating Containing Copper: A Promising Anticorrosive and Antifouling Coating for Seawater Application of AA 7075, *Surf. Coat. Technol.*, 2020, **393**(April), p 125774. <https://doi.org/10.1016/j.surfcoat.2020.125774>
 21. P. Cerchier, L. Pezzato, K. Brunelli, P. Dolcet, A. Bartolozzi, R. Bertani, and M. Dabalà, Antibacterial Effect of PEO Coating with Silver on AA7075, *Mater. Sci. Eng. C*, 2017, **75**, p 554–564. <https://doi.org/10.1016/j.msec.2017.02.084>
 22. P. Cerchier, L. Pezzato, E. Moschin, L.B. Coelho, M.G.M. Olivier, I. Moro, and M. Magrini, Antifouling Properties of Different Plasma Electrolytic Oxidation Coatings on 7075 Aluminium Alloy, *Int. Biodeterior. Biodegrad.*, 2018, **133**(June), p 70–78. <https://doi.org/10.1016/j.ibiod.2018.06.005>
 23. Y.N. Ahn, K. Do Kim, G. Anoop, G.S. Kim, and J.S. Yoo, Design of Highly Efficient Phosphor-Converted White Light-Emitting Diodes with Color Rendering Indices (R1–R15) ≥ 95 for Artificial Lighting, *Sci. Rep.*, 2019, **9**(1), p 1–10. <https://doi.org/10.1038/s41598-019-53269-0>
 24. L. Chen, C.C. Lin, C.W. Yeh, and R.S. Liu, Light Converting Inorganic Phosphors for White Light-Emitting Diodes, *Materials Basel*, 2010, **3**(3), p 2172–2195
 25. R.R. Jacobs, W.F. Krupke, and M.J. Weber, Measurement of Excited-State-Absorption Loss for Ce³⁺ in Y₃Al₅O₁₂ and Implications for Tunable 5d \rightarrow 4f Rare-Earth Lasers, *Appl. Phys. Lett.*, 1978, **33**(5), p 410–412
 26. S. Stojadinović and A. Ćirić, Sensitizing Effect of Ce³⁺ on Tm³⁺ Blue Emission in Al₂O₃:Tm³⁺/Ce³⁺ Coatings Formed by Plasma Electrolytic Oxidation, *J. Mater. Sci. Mater. Electron.*, 2021, **32**(6), p 7841–7847
 27. S. Stojadinović and A. Ćirić, Photoluminescence of ZnO:Eu³⁺ and ZnO:Tb³⁺ Coatings Formed by Plasma Electrolytic Oxidation of Pure Zinc Substrate, *J. Lumin.*, 2020, **2021**, p 235
 28. S. Stojadinović, N. Tadić, and R. Vasilčić, Down- and up-Conversion Photoluminescence of ZrO₂:Ho³⁺ and ZrO₂:Ho³⁺/Yb³⁺ Coatings Formed by Plasma Electrolytic Oxidation, *J. Alloy. Compd.*, 2019, **785**, p 1222–1232
 29. T.W. Clyne and S.C. Troughton, A Review of Recent Work on Discharge Characteristics during Plasma Electrolytic Oxidation of Various Metals, *Int. Mater. Rev.*, 2019, **64**(3), p 127–162
 30. P. Wang, Z.Y. Gong, J. Hu, J. Pu, and W.J. Cao, Effect of MgO Micro-Powder on the Characteristics of Micro-Arc Oxidation Coatings, *Surf. Eng.*, 2019, **35**(7), p 627–634. <https://doi.org/10.1080/02670844.2018.1557996>
 31. G.A. Mengesha, J.P. Chu, B.S. Lou, and J.W. Lee, Effects of Processing Parameters on the Corrosion Performance of Plasma Electrolytic Oxidation Grown Oxide on Commercially Pure Aluminum, *Metals Basel*, 2020, **10**(3), p 1–21
 32. A. Hakimzad, K. Raeissi, M.A. Golozar, X. Lu, C. Blawert, and M.L. Zheludkevich, The Effect of Pulse Waveforms on Surface Morphology, Composition and Corrosion Behavior of Al₂O₃ and Al₂O₃/TiO₂ Nano-Composite PEO Coatings on 7075 Aluminum Alloy, *Surf. Coat. Technol.*, 2017, **324**, p 208–221. <https://doi.org/10.1016/j.surfcoat.2017.05.068>
 33. P. Wang, J. Pu, X. Liu, W.J. Cao, Z.Y. Gong, J. Hu, D. Xiang, and X.Y. Guo, Characterization of Micro-Arc Oxidation Coatings on Cast Aluminum Alloy Doped with Different Y₂O₃ Particle Concentration, *Mater. Res. Express*, 2019, **6**(9), p 096544
 34. A. Longato, S. Picco, L. Moro, M. Buffolo, C. De Santi, N. Trivellini, G. Meneghesso, M. Meneghini, E. Della Gaspera, M. Guglielmi, and A. Martucci, Glass-Ceramic Composites for High-Power White-Light-Emitting Diodes, *Ceram. Int.*, 2021, **47**(13), p 17986–17992. <https://doi.org/10.1016/j.ceramint.2021.03.113>
 35. J. Chastain, J.F. Moulder, and R.C. King, Handbook of x-ray Photoelectron Spectroscopy : A Reference Book of Standard Spectra for Identification and Interpretation of XPS Data. ed by Eden Prairie, (Minnesota), Physical Electronics Division, Perkin-Elmer Corp, (1995)
 36. NIST X-ray Photoelectron Spectroscopy Database 20, Version 4.1, (2012)
 37. F. Jaspard-Mécuson, T. Czerwiec, G. Henrion, T. Belmonte, L. Dujardin, A. Viola, and J. Beauvir, Tailored Aluminium Oxide Layers by Bipolar Current Adjustment in the Plasma Electrolytic Oxidation (PEO) Process, *Surf. Coat. Technol.*, 2007, **201**, p 8677–8682
 38. C. Bertuccioli, A. Garzoni, C. Martini, A. Morri, and G. Rondelli, Plasma Electrolytic Oxidation (PEO) Layers from Silicate/Phosphate Baths on Ti-6Al-4V for Biomedical Components: Influence of Deposition Conditions and Surface Finishing on Dry Sliding Behaviour, *Coatings*, 2019, **9**(10), p 614
 39. A. Toulabifard, M. Rahmati, K. Raeissi, A. Hakimzad, and M. Santamaria, The Effect of Electrolytic Solution Composition on the Structure, Corrosion, and Wear Resistance of PEO Coatings on AZ31 Magnesium Alloy, *Coatings*, 2020, **10**(10), p 1–19
 40. A. Fattah-alhosseini, R. Chaharmahali, and K. Babaei, Effect of Particles Addition to Solution of Plasma Electrolytic Oxidation (PEO) on the Properties of PEO Coatings Formed on Magnesium and Its Alloys: A Review, *J. Magnes. Alloy.*, 2020, **8**(3), p 799–818. <https://doi.org/10.1016/j.jma.2020.05.001>
 41. S. Sikdar, P.V. Menezes, R. Maccione, T. Jacob, and P.L. Menezes, Plasma Electrolytic Oxidation (PEO) Process—Processing, Properties, and Applications, *Nanomaterials*, 2021, **11**(6), p 799
 42. M. O'Hara, S.C. Troughton, R. Francis, and T.W. Clyne, The Incorporation of Particles Suspended in the Electrolyte into Plasma Electrolytic Oxidation Coatings on Ti and Al Substrates, *Surf. Coat.*

- Technol.*, 2020, **385**(2019), p 125354. <https://doi.org/10.1016/j.surfcoat.2020.125354>
43. A.B. Rogov, H. Lyu, A. Matthews, and A. Yerokhin, AC Plasma Electrolytic Oxidation of Additively Manufactured and Cast AlSi12 Alloys, *Surf. Coat. Technol.*, 2020, **399**, p 1–14
44. V. Dehnavi, X.Y. Liu, B.L. Luan, D.W. Shoesmith, and S. Rohani, Phase Transformation in Plasma Electrolytic Oxidation Coatings on 6061 Aluminum Alloy, *Surf. Coat. Technol.*, 2014, **251**, p 106–114. <https://doi.org/10.1016/j.surfcoat.2014.04.010>
45. V. Dehnavi, D.W. Shoesmith, B.L. Luan, M. Yari, X.Y. Liu, and S. Rohani, Corrosion Properties of Plasma Electrolytic Oxidation Coatings on an Aluminium Alloy—The Effect of the PEO Process Stage, *Mater. Chem. Phys.*, 2015, **161**, p 49–58. <https://doi.org/10.1016/j.materchemphys.2015.04.058>
46. X. Lu, C. Blawert, K.U. Kainer, T. Zhang, F. Wang, and M.L. Zheludkevich, Influence of Particle Additions on Corrosion and Wear Resistance of Plasma Electrolytic Oxidation Coatings on Mg Alloy, *Surf. Coat. Technol.*, 2018, **352**(July), p 1–14. <https://doi.org/10.1016/j.surfcoat.2018.08.003>

Publisher's Note Springer Nature remains neutral with regard to jurisdictional claims in published maps and institutional affiliations.